Depth-dependent electronic states of Fe_3O_4 across the Verwey transition studied by hard x-ray photoemission spectroscopy

Shigenori Ueda[1,2*], Azusa N. Hattori[3], and Hidekazu Tanaka[3]

[1]*Research Center for Electronic and Optical Materials, National Institute for Materials Science (NIMS), Tsukuba 305-0044, Japan*

[2]*Synchrotron X-ray Station at SPring-8, NIMS, Sayo, Hyogo 679-5148, Japan*

[3]*SANKEN, The University of Osaka, Ibaraki, Osaka 567-0047, Japan*

Abstract

Depth-dependent electronic states of a prototypical strongly correlated Fe_3O_4 thin film across the Verwey transition temperature (T_V ~125 K) were investigated by hard x-ray photoemission spectroscopy (HAXPES) combined with x-ray total reflection (TR). We found that the Fe 2*p* HAXPES spectral shapes strongly depend on the effective inelastic mean-free-path (λ_{eff}) regardless of temperature (*T*). Particularly, the shoulder structure located at the lower binding energy side of the Fe $2p_{3/2}$ main peak becomes more pronounced with increasing λ_{eff}, (*i.e.*, increasing bulk sensitivity), indicating a significant difference in the electronic structures between the surface and deeper regions of the film. This trend coincides with the increase of the density of states near the Fermi-level (E_F) for larger λ_{eff}, suggesting the contribution of non-local screening effects. While the valence band spectra show a clear metal-to-insulator transition across T_V, the Fe 2*p* core-level HAXPES and the magnetic circular dichroism profiles for large λ_{eff} are almost independent on *T*. This behavior suggests that the average valence of the *B*-site Fe species is maintained at 2.5+ across T_V. Comparison with the configuration interaction theory based on the cluster model calculations

emphasizes the importance of non-local screening effects in the Fe 2*p* spectral shapes. Our results demonstrate that HAXPES combined with TR is a powerful technique for probing systematic depth-dependent electronic states. By providing this systematic dataset from the surface to deeper regions, this work serves as a reliable benchmark for the research field.

*Corresponding author. E-mail: UEDA.Shigenori@nims.go.jp

I. Introduction

Hard x-ray photoelectron spectroscopy (HAXPES) is a powerful tool for elucidating the bulk-sensitive electronic structures of solids [1-4] because of the large inelastic mean-free-path (IMFP) of photoelectrons with the kinetic energy (E_K) of several keV in solids [5]. Even in core-level photoelectron spectroscopy (PES), HAXPES can reveal bulk-derived electronic states, which are difficult to detect by surface-sensitive PES using soft x-ray (SX) light sources, in the strongly correlated electron systems [6-12]. To access both the surface- and bulk-derived (*i.e.,* depth-dependent) electronic states, the IMFP (λ_e) of photoelectrons must be tuned. This is usually achieved by varying E_K by changing the excitation photon energy ($h\nu$) [6-8,12] or varying effective λ_e (λ_{eff}) by changing the take-off angle (TOA) of photoelectrons [13-16]. In the former approach, the fact that λ_e increases with E_K [5] is exploited: by selecting different $h\nu$ one changes E_K and therefore λ_e. In the latter approach, λ_{eff} is given by $\lambda_{eff} = \lambda_e \sin(\mathrm{TOA})$, where TOA is the angle between the emitted photoelectron trajectory and the sample surface. By varying TOA, λ_{eff} can be reduced (more surface-sensitive) or increased (more bulk-sensitive), enabling systematic depth-dependent PES measurements.

Recently, a high-throughput method for probing depth-dependent electronic states has been realized by HAXPES combined with x-ray total reflection (TR). Around the TR critical angle (θ_C), λ_{eff} can be tuned in the range between ~2 and ~13 nm from the surface [17]. Using the TR-HAXPES method, the surface band bending of polar GaN was examined by measuring λ_{eff}-dependent HAXPES spectra; the relationship between λ_{eff}, λ_e, and λ_p (x-ray attenuation length) is expressed by $\lambda_{eff} = \lambda_e\lambda_p/(\lambda_e+\lambda_p)$ [17]. Recently, Mizutani *et al*. [18] demonstrated that non-TR- and TR-HAXPES can reveal the difference of the electronic states between the surface and bulk regions in the strongly correlated oxides such as $La_{0.6}Sr_{0.4}MnO_3$ and $La_{1.9}Ce_{0.1}CuO_4$. Since the surface-sensitive PES using vacuum ultraviolet (VUV) and SX light sources often yields electronic structures that contradict the

bulk physical properties of strongly correlated systems, it is essential that λ_{eff} should be sufficiently larger than the thickness of surface-affected layer, in which the electronic structure differs from bulk. By varying λ_p, the λ_{eff}-dependent HAXPES can reveal the thickness of the surface region in strongly correlated electron systems. Moreover, the spectra for the buried bulk region can be extracted numerically from the set of the λ_{eff}-dependent measurements, as described in Ref. [17].

Magnetite (Fe_3O_4) is a prototypical strongly correlated oxide, and exhibits ferrimagnetism with a very high Curie temperature (T_C) of ~860 K. Fe_3O_4 is also known as a predicted half-metal in the high-temperature (HT) phase above the Verwey transition temperature (T_V), and has attracted much attention for spintronic applications due to a possible perfect spin polarization at the Fermi-level (E_F). This perfect polarization originates from the conducting t_{2g} minority spin electrons of the octahedral *B*-site Fe [19,20]. In addition, Fe_3O_4 exhibits a metal-to-insulator transition (MIT) together with a cubic-to-monoclinic structural transition on cooling below T_V ~120 K (low-temperature (LT) phase) [21-24].

There are many PES studies on Fe_3O_4 by using a rich variety of photon sources. For the valence band (VB) measurements, $h\nu$ ranges from 4.65 eV to 8 keV [12,25-31]. For the Fe 2*p* core-level spectral measurements, $h\nu$ ranges from 800 eV to 8 keV [12,29,32-36]. In addition, magnetic circular and linear dichroism (MCD and MLD) studies in the Fe 2*p* core-level x-ray absorption spectroscopy (XAS) for Fe_3O_4 have been reported to reveal the electronic and magnetic states of Fe species in the *A*- and *B*-sites [29,37-40].

For the VB spectra of Fe_3O_4, the reported spectral features around the Fermi-level (E_F) strongly depend on $h\nu$ due to the changes in the photoionization cross-section ratio of the Fe 3*d*/O 2*p* orbitals [41], which are clearly seen in Refs. [25,28]. In addition to the spectral features around E_F regardless of $h\nu$, the conflict experimental results have been reported on MIT across T_V. Some studies report a small gap across E_F (or a spectral onset energy, E_{on}, is located below E_F) even in the HT phase as

well as the LT phase as reported in Refs. [26-28]. Other works report a clear MIT in which E_{on} is located below (above) E_F in the LT (HT) phase as reported in Refs. [12,25]. These discrepancies can be attributed to (i) variations in the surface condition of Fe_3O_4 samples, (ii) $h\nu$-dependent photoionization cross-section, and (iii) photoelectron E_K-dependent λ_e. In fact, it has been reported that the electronic states originated from bulk are strongly suppressed within a surface layer of roughly 10 nm in depth for bulk Fe_3O_4 [12].

The impact of the probing depth is clearly observed in the Fe 2*p* core-level PES of Fe_3O_4 through the TOA-dependent measurements with the Al-Kα excitation (1.48 keV) reported in Ref. [33]. In the spectrum taken at shallow TOA = 7º, the *B*-site Fe^{2+} component (the binding energy (E_B) of ~ 709 eV) is strongly reduced relative to the Fe^{3+} components (E_B of ~ 710.5 eV) when compared with the spectrum taken at a normal emission (TOA = 90º), where the Fe 2*p* core-level spectrum is considered as a sum of three distinct components of the *A*-site Fe^{3+}, *B*-site Fe^{3+}, and *B*-site Fe^{2+} , as described by the mixed valence formula of $[Fe^{3+}(\downarrow:5\mu_B)]_AO[Fe^{3+}(\uparrow:5\mu_B)Fe^{2+}(\uparrow:4\mu_B)]_BO_3$. Apart from this probing depth dependence, the mixed valence picture also accounts for the intensity variations of the *B*-site Fe^{2+} component when the tetrahedral *A*-site Fe^{3+} is partially substituted by Zn^{2+} or Mn^{2+}. In these cases, the intensity of *B*-site Fe^{2+} component diminishes to satisfy the charge neutrality of $Fe_{3-x}M_xO_4$ (*M* = Mn, Zn) [29,34,35]. In contrast, the configuration interaction theory (CI) theory based on the cluster model calculation for the Fe 2*p* core-level spectrum for Fe_3O_4 with using three distinct components (*A*-site Fe^{3+}, *B*-site Fe^{3+}, and *B*-site Fe^{2+}) tends to underestimate the intensity at E_B of ~709 eV compared with the experimental spectrum [32].

Taguchi *et al*. [12] also reported a clear λ_e-dependent Fe 2*p* core-level spectral shapes for $h\nu$ of 1.0 and 7.94 keV. The bulk-sensitive Fe 2*p* HAXPES spectrum ($h\nu$ = 7.94 keV) of Fe_3O_4 in the HT phase showed a larger intensity at E_B of ~709 eV than the surface-sensitive PES ($h\nu$ = 1.0 and 1.48 keV) [32,33]. They also reproduced the experimental HAXPES spectrum by using an extended

impurity Anderson model (IAM) with including a non-local screening effect [6-8] for two distinct *A*- and *B*-site Fe species, because all *B*-site Fe atoms in Fe_3O_4 are crystalographically equivalent in the HT phase. Although the experimental Fe 2*p* HAXPES is well reproduced by the extended IAM calculation, the MCD profiles in Fe 2*p* HAXPES spectra between the experiment and extended IAM calculation are limited to partial agreement. In contrast, the Fe 2*p* XAS-MCD and MLD of Fe_3O_4 in the HT phase have been analyzed by the CI cluster model calculations with three distinct components (*A*-site Fe^{3+}, *B*-site Fe^{3+}, and *B*-site Fe^{2+}). These CI cluster model calculations reproduce the experimental XAS-MCD and MLD spectral shapes qualitatively [39,40].

To obtain reliable surface-to-bulk electronic states of Fe_3O_4, depth-dependent VB near E_F and Fe 2*p* core-level measurements that are less affected by $h\nu$ (e.g., cross-section ratio of the Fe 3*d*/O2*p* orbitals) and experimental geometry (*e.g.*, TOA) are required. Earlier PES studies [12,25-28,30,33] reported inconsistent trends: E_{on} of Fe_3O_4 in the VB spectra near E_F varied with $h\nu$, and the intensity of the Fe 2*p* core-level component at E_B of ~709 eV changes with $h\nu$ and/or TOA. To perform the depth-dependent measurements, we utilize TR-HAXPES for an epitaxial Fe_3O_4 film sample, since λ_{eff} in HAXPES can be changed from ~2 to ~14 nm by a slight change of x-ray incidence angle (θ_{in}) between ~0.4º and 2º with respect to the sample surface; a flat sample surface is suitable for small θ_{in} due to the expansion of x-ray footprint on the surface. In this work, we investigate the temperature (*T*)- and λ_{eff}-dependent electronic states of an epitaxial Fe_3O_4(001) film on a MgO(001) substrate by the Fe 2*p* core-level and VB HAXPES measurements combined with TR, together with *T*-dependent Fe 2*p* core-level MCD-HAXPES measurements. These measurements clarify the density of states (DOS) near E_F as well as E_{on} and the Fe 2*p* HAXPES intensity at E_B of ~709 eV across T_V for various λ_{eff}.

This work provides the experimental and theoretical results of the Fe_3O_4 film by using HAXPES as follows; (i) Systematic λ_{eff}-dependent VB and Fe 2*p* core-level spectra of Fe_3O_4 by the HAXPES

measurements were performed to clarify the changes in the electronic states from the surface to deeper regions. The Fe 2*p* HAXPES spectra of the Fe_3O_4 film showed a clear enhancement of the shoulder structure located at E_B of ~709 eV as λ_{eff} increased, regardless of T. This enhancement correlated with the increase of the DOS at around E_F with λ_{eff}. (ii) A proxy measure of E_{on} of the VB near E_F as a function of depth and T suggests that the surface layer (a several nm in depth), whose electronic structure differs from deeper region, exists in the Fe_3O_4 film. (iii) In the analysis of the Fe 2*p* HAXPES spectra, we discussed the discrepancies between this work, Ref. [12], and the CI calculations by considering several possibilities such as photoelectron diffraction (PED), non-local screening effect, experimental geometry and linear dichroism in HAXPES. (iv) The CI calculations in the mixed valence model well reproduce the Fe 2*p* XMCD spectrum of Fe_3O_4 as well as the Fe 2*p* MCD spectra in HAXPES with λ_{eff} = 7.33 nm, while the experimental Fe 2*p* HAXPES and MCD profiles in HAXPES are almost unchanged across T_V. However, the discrepancy between the experimental bulk-sensitive Fe 2*p* HAXPES and calculated spectra is found in the intensity of the shoulder structure. These results provide not only the depth-dependent evolution of the core-level and VB spectra but also a reliable benchmark for understanding the electronic states across the Verwey transition and for the future studies of Fe_3O_4.

II. Experiment

A 150-nm-thick epitaxial Fe_3O_4(001) thin film was grown on a MgO(001) substrate by a pulsed-laser deposition. The film was fabricated according to the growth procedures described in Ref. [42]. The T-dependent resistivity clearly showed a sharp metal-insulator transition across T_V. The sharpness of resistivity change was almost identical to that of the 160-nm-thick film reported in Ref. [42]. In addition, T_V was approximately 125 K, which is close to the bulk value of Fe_3O_4. These results indicate that the present film exhibits bulk-like Verwey transition behavior. The HAXPES

measurements were conducted at the revolver undulator beamline BL15XU of SPring-8 [3,43]. θ_{in} of x-rays was referred to θ_C = 0.525° for bulk Fe_3O_4, which was calculated for $h\nu$ = 5.95 keV according to Ref. [44]. Here, θ_C, at which the HAXPES intensity showed maximum, was identified experimentally from the Fe 2*p* core-level intensity as a function of θ_{in} [17]. For λ_{eff}-dependent HAXPES, the horizontal linear polarized x-rays were used. For the MCD-HAXPES measurements, the horizontal linear polarized x-rays were converted to left- and right-handed circularly polarized x-rays (LCP and RCP) by using a diamond phase retarder. The sample *T* was controlled by an open-cycle He cryostat. The sample was remanently magnetized by applying a magnetic field of ~0.3 T along the [100] direction in air at room temperature. Then, the magnetized sample was introduced into an analysis chamber attached to a high-resolution electron analyzer (VG Scienta R4000). The experimental geometry was described in Refs. [3,17]. Total energy resolution, ΔE, was set to 240 meV for both the core-level and VB HAXPES measurements at $h\nu$ = 5.95 keV. E_B was referred to E_F of an evaporated Au film. Note that we did not perform any surface treatments after the sample fabrication. According to Refs. [5,44], λ_e and λ_p were calculated for bulk Fe_3O_4, and λ_{eff} was obtained for each θ_{in} [17].

III. Results

A. Fe 2*p* core-level HAXPES spectra of Fe_3O_4 thin film

Figure 1(a) shows the Fe 2*p* core-level HAXPES spectra of the Fe_3O_4 thin film measured at *T* = 300 K (above T_V) as a function of λ_{eff}. The spectra with λ_{eff} of 1.95, 3.76, and 7.33 nm were obtained at θ_{in} of 0.38, 0.51, and 2.00°, respectively. The spectrum corresponding to λ_{eff} of 12.8 nm was numerically obtained by using these three spectra according to Ref. [17] given by,

$$S_D = 2\times \lambda_{eff}(\theta_{in}=2.00°)\times S_A - 3\times \lambda_{eff}(\theta_{in}=0.51°)\times S_B + \lambda_{eff}(\theta_{in}=0.38°)\times S_C , \quad \text{Eq. (1)}$$

where S_A, S_B, and S_C represent the spectra with λ_{eff} of 7.33, 3.76, and 1.95 nm, respectively, which

were normalized by the integrated intensity after subtracting an integrated-type background. The obtained spectrum with λ_{eff} of 12.8 nm (S_D) reflects more bulk-sensitive electronic states due to the reduced surface contribution. The intensity contribution from the surface to 5 nm in depth relative to the total intensity is estimated to be 92.3% for λ_{eff} =1.95 nm, 73.6% for λ_{eff} =3.76 nm, 49.5% for λ_{eff} =7.33 nm, and 14.1% for λ_{eff} =12.8 nm. One sees that the spectral line shapes strongly depend on λ_{eff}. The intensity at around 715 and 730 eV (the higher E_B side of the Fe $2p_{3/2}$ and $2p_{1/2}$ peaks) decreases with increasing λ_{eff}, and the spectra become sharper for larger λ_{eff}. In contrast, the shoulder structure located at E_B of ~ 709 eV increases with increasing λ_{eff}. These results indicate that the electronic states within the top several-nm-thickness region of the film are different from bulk. A similar λ_e dependence of the shoulder structure at E_B of ~ 709 eV was reported previously by Taguchi *et al*. [12], where λ_e was tuned by the use of soft and hard x-rays as an excitation light source. Figures 1(b) and 1(c) show the spectra measured at T above and below T_V (150 and 110 K), respectively. Although the spectral shapes measured at T = 150 and 110 K are slightly sharper than those measured at 300 K, the changes in the spectral shapes at T = 150 and 110 K due to the variation of λ_{eff} were very similar to those at T = 300 K.

To clarify the dependence of the Fe 2p core-level HAXPES spectra on T and λ_{eff} in more detail, the spectra around the Fe $2p_{3/2}$ main peak region are enlarged as shown in Fig. 2, since the changes in the spectral shapes across T_V have been reported in the previous work [12]. Again, the shoulder structure located at E_B of ~709 eV increased with increasing λ_{eff} at each T with respect to the main peak located at E_B of ~710.5 eV, and the spectral weight shifted toward the lower E_B side with increasing λ_{eff}. In contrast, the spectral shape for 300 K was almost identical to those for 150 and 110 K for the bulk-sensitive λ_{eff} = 12.8 nm, even across T_V. In the mixed valence picture, the shoulder structure originates from the Fe^{2+} component in the B-site, whereas the main peak is a superposition of the Fe^{3+} component in both the A- and B-sites. The B-site Fe^{2+} and Fe^{3+} electrons

contribute to the electrical conductivity, while the *A*-site Fe^{3+} electrons are localized. To satisfy the charge neutrality in the metallic and insulating states of Fe_3O_4, the mean valence of Fe ions in the *B*-site must be 2.5+ regardless of *T*. This charge neutrality naturally explains why the Fe 2*p* core-level spectral shape does not change across T_V. However, one may suspect that the weak *T* dependence in the Fe 2*p* spectra arises from degraded electronic states near the surface, since no surface treatment was performed after the film fabrication. To verify whether the present film still exhibits MIT with the probing depth of HAXPES, we measured the VB spectra near E_F as described below.

B. VB HAXPES spectra of Fe_3O_4 thin film

To verify MIT of the Fe_3O_4 film across T_V, we have measured the VB HAXPES spectra near E_F at *T* = 300, 150, 110 K. The VB spectra measured at each *T* for different λ_{eff} (2.01, 4.07, and 8.15 nm) are shown in Figs. 3(a)-(c). Note that the intensity of VB is normalized by the integrated intensity of the entire VB region between 12 eV and −1 eV after subtracting an integrated-type background (not shown). The VB spectra with λ_{eff} = 14.0 nm was obtained by using Eq. (1). Then, the intensity normalized spectra were plotted in Fig. 3(a)-(c). The intensity contribution from the surface to 5 nm in depth relative to the total intensity is estimated to be 91.7% for λ_{eff} =2.01 nm, 70.8% for λ_{eff} =4.07 nm, 45.9% for λ_{eff} =8.15 nm, and 11.2% for λ_{eff} =14.0 nm. As an example, the position of E_{on}, obtained by the extrapolation of the leading edge near E_F, for λ_{eff} = 14.0 nm is indicated by the vertical bar in Figs. 3(a)-(c). Here, we define E_{on} as a proxy for the valence band maximum, although the value of E_{on} is an empirical measurement dependent on the fitting range, *T*, ΔE, and background subtraction. Note that the observed E_{on} in Fig. 3 suggests a redistribution of DOS near E_F. The dependence of E_{on} on *T* and λ_{eff} is summarized in Fig. 3(d). E_{on} above T_V shows a negative value (metallic behavior), while E_{on} below T_V shifts to a positive value, indicating the opening of bandgap across E_F. In addition, the position of E_{on} shifts to the negative energy side as

λ_{eff} increases, suggesting that deeper regions exhibit a larger metallic contribution. These results confirm that a clear MIT occurs across T_V in the present Fe_3O_4 thin film and reveal the existence of the depth-dependent electronic states in Fe_3O_4.

C. Fe 2*p* core-level MCD-HAXPES of Fe_3O_4 thin film

We have also performed the Fe 2*p* core-level MCD-HAXPES measurements at T = 300, 150, and 110 K with a fixed λ_{eff} = 7.33 nm (θ_{in} = 2.00°) [45]. Here, MCD is defined as the intensity difference between the spectra measured with RCP and LCP x-rays. It is expected that MCD is sensitive to the changes of the electronic states of Fe_3O_4 by the changes of the multiplet structures, when the *B*-site Fe electronic states are modified by MIT. Figure 4 shows the Fe 2*p* MCD-HAXPES spectra of the Fe_3O_4 thin film measured at T =300, 150, and 110 K. The MCD-HAXPES spectra of the Fe_3O_4 thin film measured at T = 300 K are similar to that reported in Ref. [34]. At first glance, the Fe 2*p* core-level HAXPES spectra measured with LCP and RCP x-rays are almost *T*-independent, and the resulting MCD profiles show no obvious *T*-dependent variation. The MCD profiles intrinsically show the complicated structures due to the superposition of contributions from the *A*- and *B*-site Fe species, which have the opposite magnetization direction, and they are further influenced by the strong electron correlation effect. Nevertheless, the overall spectral shape of MCD is almost the same at T = 300, 150, 110 K. Slightly sharper line shapes of the Fe 2*p* core-level HAXPES and MCD spectra at lower *T* are probably due to the reduction of thermal broadening effects. A similar *T* independence of the Fe 2*p* XAS and MCD spectra in Fe_3O_4 across T_V has been reported in Ref. [38]. Almost identical MCD-HAXPES spectral shapes at T = 300, 150, and 110 K suggest that the mean valence of Fe ions in the *B*-site sustains to be 2.5+ at *T* above and below T_V to satisfy the charge neutrality.

D. CI cluster model calculations for Fe_3O_4

To understand the electronic states of Fe species in the *A*- and *B*-sites from the Fe 2*p* core-level MCD-HAXPES spectra, we have performed the CI cluster model calculations with full multiplets by using a software of CTM4XAS [46]. The complicated MCD profile observed in the HAXPES spectra can be a fingerprint of the electronic states of Fe_3O_4. We have also calculated the XAS-MCD for the Fe 2*p* core-level to confirm the reliability of the used electronic structure parameter set, which reproduces the experimental MCD-HAXPES spectra. In the calculations, the basis states for the *B*-site Fe^{2+} are chosen to $3d^6$, $3d^7\underline{L}$, and $3d^8\underline{L}^2$, where $\underline{L}$ denotes the ligand O 2*p* hole. The basis states for the *A*- and *B*-site Fe^{3+} are chosen to $3d^5$, $3d^6\underline{L}$, and $3d^7\underline{L}^2$. The charge transfer energy (Δ) is defined as $E(3d^{n+1}\underline{L}) - E(3d^n)$, where n is 5 and 6 for Fe^{3+} and Fe^{2+}, respectively. The electronic structure parameters of the crystal field splitting (10*Dq*), Fe 3*d*-3*d* (2*p*-3*d*) Coulomb interaction (U_{dd} (U_{dc})), and hybridization strength between the Fe 3*d* (e_g and t_{2g}) and ligand O 2*p* states ($V(e_g)$ and $V(t_{2g})$, respectively) are taken into account in the calculations.

Figures 5(a)-5(c) show the site-resolved MCD-HAXPES spectra calculated for the Fe 2*p* core-level region of Fe_3O_4; the *B*-site Fe^{2+} component in Fig. 5(a), the *B*-site Fe^{3+} component in Fig. 5(b), and the *A*-site Fe^{3+} component in Fig. 5(c). These calculations were performed with the electronic structure parameter set listed in Table I. Figure 5(d) shows the sum of the three site-dependent spectra. The relative spectral weights of the *B*-site Fe^{2+} and Fe^{3+} and *A*-site Fe^{3+} contributions are set to 1 : 1 : 1. An integrated-type background was added to the RCP- and LCP-HAXPES spectra in Fig. 5(d) for comparison with the experimental spectra in Fig. 4. One sees that the calculated LCP- and RCP-HAXPES and MCD spectra (Fig. 5(d)) are similar to the experimental ones (Fig. 4), while the shoulder structure located at E_B of ~709 eV in the calculated LCP spectrum is weaker than the experimental one. Figure 5(e) compares the MCD profile obtained from the calculation with the measured MCD spectra at T = 300, 150, and 110 K. One sees that the calculated MCD profile

reproduces well the complicated MCD profiles in the experiments. This result again suggests that the mean valence of Fe ions in the *B*-site sustains to be 2.5+ at *T* above and below T_V. Using the same parameter set listed in Table I, we have calculated the Fe 2*p* core-level XAS and MCD spectra as shown in Fig. 6. The calculated RCP- and LCP-XAS and MCD spectra also reproduce well the previously reported experimental data for Fe_3O_4 [29,38,39]. Thus, we were able to obtain the reliable electronic parameter set for Fe_3O_4 from the CI cluster model calculations using the *B*-site Fe^{2+} and Fe^{3+}, and *A*-site Fe^{3+} components.

IV. Discussion

A. Depth-dependent Fe 2*p* spectra and VB spectra near E_F

Let us consider a possible origin of the depth-dependent electronic states of Fe_3O_4. As shown in Figs. 2(a)-(c), the intensity of the shoulder structure at E_B ~709 eV in the Fe 2*p* HAXPES spectra increases with increasing λ_{eff} at each *T*. Simultaneously, the intensity of VB near E_F (in other words, DOS) increases with λ_{eff} as shown in Figs. 3(a)-(c). This correlation indicates that the intensity of the shoulder structure is affected by the non-local screening effect through the hybridization between the coherent and Fe 3*d* states as reported in strongly correlated systems in HAXPES [6-8]. The depth- and *T*-dependent E_{on} in Fig. 3(d) clearly shows that E_{on} shifts toward the positive energy side with decreasing λ_{eff}. Although the *T*-dependent E_{on} for λ_{eff} = 8.15 and 14.0 nm clearly shows the MIT behavior, E_{on} for λ_{eff} = 2.01 and 4.07 nm at *T* = 150 K is located at ~E_F even above T_V. A similar *T*-dependence of E_{on} for λ_{eff} = 2.01 and 4.07 nm suggests that the electronic structure of surface region (at least several nm in depth) differs from the deeper region.

For the VB PES studies on bulk single crystal Fe_3O_4 [12,25-28], a clean surface is obtained by *in situ* fracture or cleavage for various surface orientations without post annealing. In these works, inconsistent results on E_{on} across T_V has been reported; (i) the presence of MIT for the cleaved surface

of bulk Fe_3O_4(110) is found in VUV-PES [25], (ii) the bandgap is opened in both the LT and HT phase for the cleaved (001) surface in SX-PES [26], (iii) the changes in E_{on} around T_V are varied for the annealed surfaces in the polished (111) and (100) surfaces and fractured surface in SX-PES [27], and (iv) in the HAXPES studies [12,28], MIT is observed for the fractured surfaces, but E_{on} at 150 K (HT phase) in Ref. [28] shows the positive value (presence of bandgap). These discrepancies are probably caused by that fracture- or cleavage-induced strain remains near the surface region, since for high-quality sample to obtain, pieces of Fe_3O_4 single crystal are annealed in an atmosphere of mixture of CO and CO_2 to release internal strain and to homogenize the composition after cutting the ingot into pieces [47,48].

For the *in situ* grown epitaxial (111) thin film reported in Ref. [33], the photoelectron diffraction (PED) analysis suggested the interlayer spacing in top five atomic layers deviates from the bulk value by -57 ~ +29%. Therefore, structural relaxation near the surface is expected even for epitaxial films. In the present epitaxial (001) film, the broader Fe 2*p* spectra λ_{eff} = 1.95 and 3.76 nm compared with those for larger λ_{eff} seen in Fig. 1 may reflect modifications of the local electronic environment of Fe species near the surface. From these results, together with the systematic λ_{eff}-dependent changes in E_{on}, DOS near E_F, and Fe 2*p* shoulder intensity, we can conclude that the near-surface electronic states of Fe_3O_4 differ from the bulk electronic states over a depth scale of several nanometers. Note that the observed differences between the surface- and bulk-sensitive spectra may be influenced by not only surface relaxation and but also potential variations in surface stoichiometry or adsorbates/contaminations in the film surface due to the exposure to air. In the following subsections, we will discuss the weaker shoulder intensity in Fe 2*p* HAXPES spectra with λ_{eff} =12.8 nm compared with the spectra reported in Ref. [12].

B. Effect of experimental geometry and linear dichroism in Fe 2*p* spectra

In our measurements, the photoelectrons approximately emitted along the [001] direction of the

Fe_3O_4 film were measured, since the grazing incidence with nearly normal emission geometry was adapted [3,17]. In contrast, for bulk Fe_3O_4 in Ref. [12], the nominal surface orientation and detailed experimental geometry were not explicitly described. Therefore, differences in the experimental geometry may partly contribute to the discrepancy in the Fe 2*p* HAXPES spectral shapes between this work and Ref. [12]. Mori *et al*. [49] reported that, in the single crystal case, the detection-direction of photoelectrons can induce linear dichroism in HAXPES (LD-HAXPES), which appears as changes in spectral shapes depending on the emission-direction of photoelectrons. This effect is clearly observed in the core-level region for Yb compounds, which reflects the asymmetric electron occupation in the 4*f* orbital. In the case of Fe_3O_4, the *B*-site Fe^{3+} has the $3d^5$ high spin configuration (half-filled, symmetric). In contrast, the *B*-site Fe^{2+} has the $3d^6$ high spin configuration (five majority spin electrons and one t_{2g} minority spin electron), which can lead to an asymmetric 3*d* occupation. The dominant difference in the Fe 2*p* HAXPES spectra between this work and Ref. [12] is found in the shoulder structure at E_B of ~709 eV, which is originated from the *B*-site Fe^{2+} in the mixed valence picture. Therefore, one may consider that geometry-dependent LD effect can partly influence the shoulder intensity. However, Sekiyama *et al*. [50] reported that LD is absent in principle for the *p* core-level photoemission from localized ions in a cubic symmetry. Since the metallic HT phase of Fe_3O_4 is cubic, LD-HAXPES cannot explain the observed discrepancy. On the other hand, MLD in core-level HAXPES, which is the intensity difference between the magnetizations parallel and perpendicular to the ***E***-vector of x-rays, has been reported by Stryganyuk *et al*. [51]. In bulk Fe_3O_4, the predominant cleave plane is known to be {111}, whereas the nominal surface of bulk Fe_3O_4 is not given in Ref. [12]. If the nominal surface in Ref. [12] is close to (111), relative relationship between the easy magnetization axis and the ***E***-vector could differ from that in this work. Therefore, the MLD contribution to the shoulder intensity could not be ignored.

C. Effect of PED

Even if the LD or MLD contribution is small, the detection-direction influences the relative intensity ratio of *A*- and *B*-site contribution via the PED effect. Hashimoto *et al*. [36] reported the site-selective core-level PES for Fe_3O_4 using PED along the [001] and [113] directions by SX-PES and HAXPES. In their work, the core-level spectrum in SX-PES for the [001] direction showed the higher *B*-site sensitivity, whereas that for the [113] direction was sensitive to the *A*-site. Their results were consistent with the simulations of the photoemission intensity angular distribution (PIAD) for SX-PES. For HAXPES, the Fe 2*p* core-level spectra measured along the [001] and [113] directions showed a weaker site-selectivity than SX-PES spectra. These results were also reproduced by their PIAD simulations and were understood by the direction of forward focusing peaks (FFPs) in PIAD from each site. We also performed the PIAD calculations for the 2*p* photoelectrons with E_K = 5240 eV according to Ref. [52] and compared the [001] and [111] FFPs for the (001) and (111) surfaces, respectively (not shown). We found that the *B*-site intensity for the [001] FFP is enhanced by a factor of 1.3 relative to that for the *A*-site with considering the acceptance angle of the electron analyzer (±7°). Here the factor was already divided by 2 due to the site occupancy ratio of the *B*/*A* sites. In contrast, the *B* site-intensity reduces to 80% for the [111] FFP in the same condition. Although the site-selectivity is weak in PED in HAXPES compared to SX-PES, our PED calculations indicate that FFP peaks can slightly modify the Fe 2*p* spectral shape. Bulk-sensitive core-level HAXPES with higher site-selectivity helps to reveal the site-specific spectral shapes. We considered that comparison of the experimental site-specific Fe 2*p* spectra with the CI and extended IAM calculations for the selective Fe 2*p* spectra gains insights into the bulk electronic states of Fe_3O_4. To do so, x-ray standing-wave (XSW) HAXPES [53] will be useful, but ultrahigh-quality bulk single crystal is required.

D. Limitation of the CI cluster model

In the analysis of the experimental Fe 2*p* core-level MCD-HAXPES spectra of Fe_3O_4, we used the CI cluster model calculations using the three distinct Fe species, *i.e.*, the *A*-site Fe^{3+}, *B*-site Fe^{2+}, and *B*-site Fe^{3+}, for simplicity. This approach has been widely used in the analysis of the Fe 2*p* PES and XAS-MCD spectra for Fe_3O_4 [32,37-39,54] as mentioned above. Although the calculated MCD profile in Fig. 5(e) reproduces the experimental profiles at T = 300, 150 and 110 K, the shoulder structure at E_B of ~709 eV in the calculated LCP spectrum in Fig. 5(d) is noticeably weaker than the experimental ones in Fig. 4. The discrepancy becomes even more evident when the LCP and RCP spectra are summed as shown in Fig. 7. This problem has been pointed out by Taguchi *et al*. [12]. To overcome this problem in the calculations, they treated the *B*-site Fe as not two distinct species but one species, because the *B*-site of Fe ions are crystallographically equivalent at T above T_V [55,56]. Their extended IAM introduces the charge transfer between the Fe 3*d* orbital and coherent state in the *B*-site Fe species, which enhances the well-screened shoulder structure. That is, the shoulder structure cannot be explained by the *B*-site Fe^{2+} in the simple mixed valence picture. Therefore, the shoulder structure at E_B ~709 eV is partly caused by the well-screened states for the *B*-site Fe species through the charge transfer from the coherent to the Fe t_{2g} minority spin states (*i.e.*, the non-local screening effect) in the photoemission final states, while the main peak at E_B ~710.5 eV mainly arises from both the poorly-screened states for the *B*-site Fe in the final states and the *A*-site Fe^{3+}. Thus, we can conclude that the non-local screening effect enhances the intensity of the shoulder structure in the bulk-sensitive Fe 2*p* HAXPES spectra of the Fe_3O_4 thin film. Again, the site-selective Fe 2*p* HAXPES measurements are needed to correctly understand the electronic structure of Fe_3O_4 from the extended AIM calculations.

E. Non-local screening and trimeron in the LT phase

Below T_V, the crystal symmetry of Fe_3O_4 changes from a cubic to monoclinic, and the *B*-site Fe species exhibit a complex charge-orbital order with 16 nonequivalent Fe ionic states based on the valence bond sum analysis [57]. This complex structure is formed by the network of trimerons [57-59], in which each trimeron consists of three linear Fe ions in the nearest neighboring *B*-site. As seen in Figs. 1 and 2, for the more bulk-sensitive spectra (λ_{eff} =12.8 nm), the intensity of the shoulder structure at E_B ~709 eV measured at T = 110 K (below T_V) is comparable to those measured at T = 300 and 150 K (above T_v). This result indicates that even in the insulating state, the similar core-hole screening process via the t_{2g} minority spin electron near E_F at the *B*-site exists in the photoemission final states, which can be explained by the charge transfer of the t_{2g} minority spin electron within the trimerons [57] and/or the sliding motion of the trimerons [58]. In the extended IAM calculation of the Fe 2*p* HAXPES spectrum for the insulating phase [12], the *B*-site Fe species were treated by three distinct $Fe^{2.4\text{-}2.5+}$-like, $Fe^{\sim 2.7+}$-like, and $Fe^{2.8\text{-}2.94+}$-like ion species to emulate 16-nonequivalent Fe ionic states. The calculated spectrum reproduced the experimental spectrum for the insulating state, when the coherent state near E_F in the insulating state was assumed as well as the metallic state due to the very small spectral change in the intensity near E_F across T_V measured by HAXPES [12]. Thus, we can conclude that even in the insulating state of Fe_3O_4, the shoulder structure at E_B of ~709 eV in the Fe 2*p* HAXPES spectrum with λ_{eff} = 12.8 nm is partly caused by the non-local screening effect at the *B*-site Fe species via the charge transfer of the t_{2g} minority spin electron inside the trimerons. However, the different trend in the shoulder structure across T_V between this work and Ref. [12] remains unresolved; weak LD caused by the monoclinic distortion may play a role.

F. MCD-HAXPES versus XAS-MCD

The experimental MCD profiles in Fe 2*p* HAXPES are well reproduced by the CI cluster model

calculations (Fig. 5(e)) by using the electronic structure parameter set listed in Table I. The same parameters set also yields XAS-MCD spectra (Fig. 6) that agree with the reported spectra [29,38,39]. The key difference between PES and XAS final states lies in the screening channel. XAS creates a 2*p* photo-hole and simultaneously promotes an electron into unoccupied 3*d* states, that is, the system remains charge neutral in the XAS final states. The excited electron in the unoccupied 3*d* states contributes to the photo-hole screening, and there is a little room for the contribution of the additional screening via the charge transfer. In contrast, PES creates a 2*p* photo-hole and ejects one photoelectron, that is, the transition from N to N–1 electron system. In this case, there is room for the photo-hole screening via the charge transfer process due to the local and non-local screening effects. Therefore, the non-local screening that enhances the shoulder structure at E_B of ~709 eV is significant for HAXPES, but only marginally affects XAS-MCD. Although the MCD profiles in Fe 2*p* HAXPES and Fe 2*p* XAS are well reproduced by the CI calculations, it is unclear whether the non-local screening and PED effects modify the MCD profile in Fe 2*p* HAXPES. Thus, we conclude that the theoretical approach including the non-local screening and PED effects for the Fe 2*p* MCD-HAXPES and the experimental site-selective Fe 2*p* MCD-HAXPES spectra with high bulk-sensitivity are required to fully understand the nature of the Fe 2*p* HAXPES spectra for Fe_3O_4.

V. Summary

T- and λ_{eff}-dependent VB and Fe 2*p* core-level HAXPES measurements were performed to clarify the electronic states of the Fe_3O_4 thin film across T_V. The correlation between the shoulder structure in the Fe 2*p* spectra and DOS near E_F suggests the depth-dependent evolution of the non-local screening from the surface to deeper regions. The position of E_{on} clearly showed MIT across T_V, and E_{on} shifted to the higher E_B side with decreasing λ_{eff} at each T. Thus, we can conclude that the electronic states of the surface region (at least several nm in depth) differ from the deeper region in

the Fe_3O_4 film.

The Fe 2*p* MCD-HAXPES measurements showed the complicated structure, but were almost independent on *T*. *T*-independent behavior in the MCD profiles as well as the Fe 2*p* HAXPES spectral shapes is considered to arise from that the mean valence of *B*-site Fe species sustains to be 2.5+ across T_V, which is related to small changes in the electronic states near E_F by MIT in Fe_3O_4, while a complex charge-orbital ordered state is formed in the LT phase. The experimental MCD profile was well reproduced by the CI cluster model calculations that employ three distinct Fe species (*A*-site Fe^{3+}, *B*-site Fe^{3+}, and *B*-site Fe^{2+}) and the parameter set listed in Table I, while the CI calculations underestimated the shoulder intensity in the bulk-sensitive HAXPES spectra. These results suggest the importance of the non-local screening effect in the bulk-sensitive Fe 2*p* HAXPES spectral shapes, while it is unclear whether these effects modify the MCD profile in HAXPES. To clarify the discrepancy between the experiments and calculations, the site-selective observation of the Fe 2*p* MCD-HAXPES spectra is important to distinguish between the *A*- and *B*-site electronic states across T_V. The comparison of the experimental site-selective Fe 2*p* spectra with the theoretical approach including the non-local screening and PED effects for the Fe 2*p* MCD-HAXPES can gain insights into the bulk electronic states of Fe_3O_4 across T_V. In the experimental approach, XSW-HAXPES for the Fe 2*p* core-level is expected to be useful for the site-selective spectral observations.

Our systematic depth-dependent HAXPES measurements demonstrate that the electronic structure of the surface region differs from that in the deeper region in Fe_3O_4 and highlight the importance of the non-local screening effect. Although the observed features are broadly consistent with earlier HAXPES results, this work provides a systematic dataset obtained under a unified experimental framework from the surface to deeper regions. These results provide a reliable benchmark for understanding the electronic states across the Verwey transition and for the future

studies of Fe_3O_4.

Acknowledgements

The HAXPES measurements were performed with the approval of NIMS Synchrotron X-ray Station (Proposal No. 2016B4606). A part of this work was supported by the Tokodai Institute of Elemental Strategy (TIES: Grant No. JPMXP0112101001) and Data Creation and Utilization Type Material Research and Development Project (Grant No. JPMXP1122683430) from the Ministry of Education, Culture, Sports, Science and Technology (MEXT), Japan.

References

[1] Y. Takata, M. Yabashi, K. Tamasaku, Y. Nishino, D. Miwa, T. Ishikawa, E. Ikenaga, K. Horiba, S. Shin, M. Arita, K. Shimada, H. Namatame, M. Taniguchi, H. Nohira, T. Hattori, S. Sodergren, B. Wannberg, and K. Kobayashi, Development of hard X-ray photoelectron spectroscopy at BL29XU in SPring-8, Nucl. Instrum. Methods Phys. Res. Sect. A **547**, 50 (2005).

[2] K. Kobayashi, M. Yabashi, Y. Takata, T. Tokushima, S. Shin, K. Tamasaku, D. Miwa, T. Ishikawa, H. Nohira, T. Hattori, Y. Sugita, O. Nakatsuka, S. Sakai, and S. Zaima, High resolution-high energy x-ray photoelectron spectroscopy using third-generation synchrotron radiation source, and its applicaton to Si-high *k* insulator systems, Appl. Phys. Lett. 83, 1005 (2003).

[3] S. Ueda, Application of hard X-ray photoelectron spectroscopy to electronic structure measurements for various functional materials, J. Electron Spectrosc. Rel. Phenom. **190**, 235 (2013).

[4] C. S. Fadley, Hard X-ray photoemission with angular resolution and standing-wave excitation, J. Electron Spectrosc. Rel. Phenom. **190**, 165 (2013).

[5] S. Tanuma, C. J. Powell, and D. R. Penn, Calculations of electron inelastic mean free paths. V. Data for 14 organic compounds over the 20-2000 eV range, Surf. Intef. Anal. 121, 165 (1994).

[6] M. Taguchi, A. Chainani, K. Horiba, Y. Takata, M. Yabashi, K.Tamasaku, Y. Nishino, D. Miwa, T. Ishikawa, T. Takeuchi, K.Yamamoto, M. Matsunami, S. Shin, T. Yokoya, E. Ikenaga, K. Kobayashi, T. Mochiku, K. Hirata, J. Hori, K. Ishii, F. Nakamura, and T. Suzuki, Evidence for suppressed screening on the surface of high temperature $La_{2-x}Sr_xCuO_4$ and $Nd_{2-x}Ce_xCuO_4$ superconductors, Phys. Rev. Lett. **95**, 177002 (2005).

[7] M. Taguchi, A. Chainani, N. Kamakura, K. Horiba, Y. Takata, M. Yabashi, K. Tamasaku, Y. Nishino, D. Miwa, T. Ishikawa, S. Shin, E. Ikenaga, T. Yokoya, K. Kobayashi, T. Mochiku, K. Hirata, and K. Motoya, Bulk screening in core-level photoemission from Mott-Hubbard and charge transfer systems, Phys. Rev. B **71**, 155102 (2005).

[8] K. Horiba, M. Taguchi, A. Chainani, Y. Takata, E. Ikenaga, D.Miwa, Y. Nishino, K. Tamasaku, M. Awaji, A. Takeuchi, M.Yabashi, H. Namatame, M. Taniguchi, H. Kumigashira, M.Oshima, M. Lippmaa, M. Kawasaki, H. Koinuma, K. Kobayashi, T. Ishikawa, and S. Shin, Nature of the well screened state in hard X-ray Mn 2*p* core-level photoemission measurements of $La_{1-x}Sr_xMnO_3$ films, Phys. Rev. Lett. **93**, 236401 (2004).

[9] K. Horiba, A. Maniwa, A. Chikamatsu, K. Yoshimatsu, H. Kumigashira, H. Wadati, A. Fujimori, S. Ueda, H. Yoshikawa, E. Ikenaga, J. J. Kim, K. Kobayashi, and M. Oshima, Pressure-induced change in the electronic structure of epitaxially strained $La_{1-x}Sr_xMnO_3$ thin films, Phys. Rev. B **80**, 132406 (2009).

[10] H. Tanaka, Y. Takata, K. Horiba, M. Taguchi, A. Chainani, S. Shin, D. Miwa, K. Tamasaku, Y. Nishino, T. Ishikawa, E. Ikenaga, M. Awaji, A. Takeuchi, T. Kawai, and K. Kobayashi, Electronic structure of strained $(La_{0.85}Ba_{0.15})MnO_3$ thin films with room-temperature ferromagnetism investigated by hard x-ray photoemission spectroscopy, Phys. Rev. B **73**, 094403 (2006).

[11] S. Ueda, H. Tanaka, E. Ikenaga, J. J. Kim, T. Ishikawa, T. Kawai, and K. Kobayashi, Mn 2*p* core-level spectra of $La_{1-x}Ba_xMnO_3$ thin films using hard x-ray photoelectron spectroscopy : Relation between electronic and magnetic states, Phys. Rev. B **80**, 092402 (2009).

[12] M. Taguchi, A. Chainani, S. Ueda, M. Matsunami, Y. Ishida, R. Eguchi, S. Tsuda, Y. Takata, M. Yabashi, K. Tamasaku, Y. Nishino, T. Ishikawa, H. Daimon, S. Todo, H. Tanaka, M. Oura, Y. Senba, H. Ohashi, and S. Shin, Temperature dependence of magnetically active charge excitations in magnetite across the Verwey transition, Phys. Rev. Lett. **115**, 256405 (2015).

[13] G. Panaccione, F. Offi, P. Torelli, G. Vanko, O. Tjernberg, P. Lacovig, A. Guarino, A. Fondacaro, A. Nigro, M. Sacchi, N. B. Brooles, and G. Monaco, Analysis of surface-bulk screening competition in the electron-doped $Nd_{2-x}Ce_xCuO_4$ cuprate using x-ray photoemission spectroscopy, Phys. Rev. B 77, 125133 (2008).

[14] T. Doi, K. Kitamura, Y. Nishiyama, N. Otsuka, T. Kudo, M. Sato, E. Ikenaga, S. Ueda, and K. Kobayashi, Analysis of Cu segregation to oxide-metal interface of Ni-based alloy in a metal-dusting environment, Surf. Intef. Anal. 40, 1374 (2008).

[15] T. Nagata, J. Volk, Y. Yamashita, H. Yoshikawa, M. Haemori, R. Hayakawa, M. Yoshitake, S. Ueda, K. Kobayashi, and C. Chikyow, Interface structure and the chemical states of Pt film on polar-ZnO single crystal, Appl. Phys. Lett. 94, 221904 (2009).

[16] E. Ikenaga, M. Kobata, H. Matsuda, T. Sugiyama, H. Daimon, and K. Kobayashi, Development of high lateral and wide angle resolved hard X-ray photoemission spectroscopy at BL47XU in SPring-8, J. Electron Spectrosc. Rel. Phenom. **190**, 180 (2013).

[17] S. Ueda, Depth-resolved electronic structure measurements by hard X-ray photoemission combined with X-ray total reflection: Direct probing of surface band bending of polar GaN, Appl. Phys. Express **11**, 105701 (2018).

[18] T. Mizutani, S. Tanaka, T. Saze, K. Fujii, H. Matsuoka, M. Nakano, H. Wadati, M. Kitamura, K. Horiba, Y. Iwase, H. Kumigashira, M. Yoshiki, and M. Taguchi, Total reflection hard x-ray photoelectron spectroscopy: Applications to strongly correlated electron systems, Phys. Rev. B **103**, 205113 (2021).

[19] A. Yanase and K. Siratori, Band structure in the high temperature phase of Fe_3O_4, J. Phys. Soc. Jpn. **53**, 312 (1984).

[20] Z. Zhang and S. Satpathy, Electron states, magnetism, and the Verwey transition in magnetite, Phys. Rev. B **44**, 13319 (1991).

[21] E. J. W. Verwey, Electronic conduction of magnetite (Fe_3O_4) and its transition point at low temperatures, Nature (London) **144**, 327 (1939).

[22] M. Izumi, T. F. Koetzle, G. Shirane, S. Chikazumi, M. Matsui, and S. Todo, Structure of magnetite (Fe_3O_4) below the Verwey transition temperature, Acta Crystallogr. Sect. B **38**, 2121 (1982).

[23] J. P. Wright, J. P. Attfield, and P. G. Radaelli, Long range charge ordering in magnetite below the Verwey transition, Phys. Rev. Lett. **87**, 266401 (2001).

[24] J. Blasco, J. Garcia, and G. Subias, Structural transformation in magneite below the Verwey transition, Phys. Rev. B **83**, 104105 (2011).

[25] A. Chainani, T. Yokoya, T. Morikawa, T. Takahashi, and S. Todo, High-resolution photoemission spectroscopy of the Verwey transition in Fe_3O_4, Phys. Rev. B 51, 17976 (1995).

[26] J.-H. Park, L. H. Tjeng, J. W. Allen, P. Metcalf, and C. T. Chen, Single-particle gap above the Verwey transition in Fe_3O_4, Phys. Rev. B **55**, 12813 (1997).

[27] D. Schrupp, M. Sing, M. Tsunekawa, H. Fujiwara, S. Kasai, A. Sekiyama, S. Suga, T. Muro, V. A. M. Brabers, and R. Claessen, High-energy photoemission on Fe_3O_4: Small polaron physics and the Verwey transition, Europhys. Lett. **70**, 789 (2005).

[28] M. Kimura, H. Fujiwara, A. Sekiyama, J. Yamaguchi, K. Kishimoto, H. Sugiyama, G. Funabashi, S. Imada, S. Iguchi, Y. Tokura, A. Higashiya, M. Yabashi, K. Tamasaku, T. Ishikawa, T. Ito, S. Kimura, and S. Suga, Polaronic behavior of photoelectron spectra of Fe_3O_4 revealed by both hard X-ray and extremely low energy photons, J. Phys. Soc. Jpn. **79**, 064710 (2010).

[29] J. Takaobushi, M. Ishikawa, S. Ueda, E. Ikenaga, J-. J. Kim, M. Kobata, Y. Takeda, Y. Saitoh, M. Yabashi, Y. Nishino, D. Miwa, K. Tamasaku, T. Ishikawa, I. Satoh, H. Tanaka, K. Kobayashi, and T. Kawai, Electronic structure of $Fe_{3-x}M_xO_4$ (M = Mn,Zn) spinel oxide thin films investigated by x-ray photoemission spectroscopy and x-ray magnetic circular dichroism, Phys. Rev. B **76**, 205108 (2007).

[30] W. Wang, J.-M Mariot, M. C. Richter, O. Heckmann, W. Ndiaye, P. De Padova, A. Taleb-Ibrahimi, P. Le Fevre, F. Bertran, F. Bondino, E. Magnano, J. Krempasky, P. Blaha, C. Cacho, F. Parmigiani, and K, Hricovini, Fe t_{2g} band dispersion and spin polarization in thin films of Fe_3O_4(001)/MgO(001): Half-metallicity of magnetite revisited, Phys. Rev. B **87**, 085118 (2013).

[31] M. Schmitt, O. Kirilmaz, S. Chernov, S. Babenkov, D. Vasilyev, O. Fedchenko, K. Medjanik, Yu. Matveyev, A. Gloskovskii, C. Schlueter, A. Winkelmann, L. Dudy, H.-J. Elmers, G. Schonhense, M. Sing, and R. Claessen, Bulk spin polarization of magnetite from spin-resolved hard x-ray photoelectron spectroscopy, Phys. Rev. B **104**, 045129 (2021).

[32] T. Fujii, F. M. F. de Groot, G. A. Sawatzky, F. C. Voogt, T. Hibma, and K. Okada, *In situ* XPS analysis of various iron oxide films grown by NO_2-assisted molecular-beam epitaxy, Phys. Rev. B **59**, 3195 (1999).

[33] S. A. Chambers, S. Thevuthasan, S. A. Joyce, Surface structure of MBE-grown Fe_3O_4(001) by X-ray photoelectron diffraction and scanning tunneling microscopy, Surf. Sci. **450**, L273 (2000).

[34] S. Ueda, H. Tanaka, J. Takaobushi, E. Ikenaga, J-. J. Kim, M. Kobata, T. Kawai, H. Osawa, N. Kawamura, M. Suzuki, and K. Kobayashi, Hard X-ray photoemission spectroscopy combined with magnetic circular dichroism: Application to $Fe_{3-x}Zn_xO_4$ spinel oxide thin films, Appl. Phys. Express **1**, 077003 (2008).

[35] J. Takaobushi, H. Tanaka, T. Kawai, S. Ueda, J-. J. Kim, M. Kobata, E. Ikenaga, M. Yabashi, K. Kobayashi, Y. Nishino, D. Miwa, K. Tamasaku, and T. Ishikawa, $Fe_{3-x}Zn_xO4$ thin film as tunable high Curie temperature ferromagnetic semiconductor, Appl. Phys. Lett. **89**, 242507 (2006).

[36] Y. Hashimoto, M. Taguchi, S. Fukami, H. Momono, T. Matsushita, H. Matsuda, F. Matsui, and H. Daimon, Site-selective X-ray photoelectron spectroscopy of Fe_3O_4 by photoelectron diffraction, Surf. Interface Anal. **51**, 115 (2019).

[37] P. Kuiper, B.G. Searle, L.-C. Duda, R.M. Wolf, and P.J. van der Zaag, Fe $L_{2,3}$ linear and circular magnetic dichroism of Fe_3O_4, J. Electron Spectrosc. Rel. Phenom. **86**, 107 (1997).

[38] E.J. Goering, M. Lafkioti, S. Gold, and G. Schuetz, Absorption spectroscopy and XMCD at the Verwey transition of Fe_3O_4, J. Magn. Magn. Mater. **310**, e249 (2007).

[39] C. F. Chang, Z. Hu, S. Klein, X. H. Liu, R. Surarto, A. Tanaka, J. C. Cezar, N. B. Brookes, H.-J.

Lin, H. H. Hsieh, C. T. Chen, A. D. Rata, and L. H. Tjeng, Dynamic atomic reconstruction: How Fe_3O_4 thin films evade polar catastrophe for epitaxy, Phys. Rev. X 6, 041011 (2016).

[40] H. Elnaggar, R. Wang, M. Ghiasi, M. Yanez, M. U. Delgado-Jaime, M. H. Hamed, A. Juhin, S, S. Dhesi, and F. de Groot, Probing the local distortion of Fe sites in Fe_3O_4 thin films using enhanced symmetry selection in XMLD, Phys. Rev. Mater. **4**, 024415 (2020).

[41] J. J. Yeh, I. Lindau, Atomic subshell photoionization cross sections and asymmetry parameters: $1 \leq Z \leq 103$, At. Data Nucl. Data Tables **32**, 1 (1985).

[42] K. Fujiwara, S. Tsubota, and H. Tanaka, Improving resistance change with temperature and thermal stability in Fe_3O_4 films for high-temperature resistors, Appl. Phys. Express. **12**, 011003 (2019).

[43] S. Ueda, Y. Katsuya, M. Tanaka, H. Yoshikawa, Y. Yamashita, S. Ishimaru, Y. Matsushita, and K. Kobayashi, Present status of the NIMS contract beamline BL15XU at SPring-8, AIP Conf. Proc. **1234**, 403 (2010).

[44] B. L. Henle, E. M. Gullikson, and J. C. Davis, X-ray interactions: Photoabsorption, scattering, transmission, and reflection at E = 50-30,000 eV, Z = 1-92, At. Data Nucl. Data Tables **54**, 181 (1993).

[45] Since the remanent to saturation magnetization (M_R/M_S) ratio is ~0.3 in the film sample, the MCD-HAXPES experiments at lower θ_{in}, which expands the footprint of x-rays on the sample, involve many magnetic domains with different magnetization directions, leading to the reduction of the MCD signals. Therefore, we do not discuss the magnitude of the MCD signal at each *T*.

[46] E. Stavitski and F. M. F. de Groot, The CTM4XAS program for EELS and XAS spectral shape analysis of transition metal L edges, Micron **41**, 687 (2010).

[47] S. Todo, K. Siratori, and S. Kimura, Transport Properties of the High Temperature Phase of Fe_3O_4, J. Phys. Soc. Jpn. **64**, 2118 (1995).

[48] S. Todo, N. Takeshita, K. Kanehara, T. Mori, and N. Mori, Metallization of magnetite (Fe_3O_4)

under high pressure, J. Appl. Phys. **89**, 7347 (2001).

[49] T. Mori, S. Kitayama, Y. Kanai, S. Naimen, H. Fujiwara, A. Higashiya, K. Tamasaku, A. Tanaka, K. Terashima, S. Imada, A. Yasui, Y. Saitoh, K. Yamagami, K. Yano, T. Matsumoto, T. Kiss, M. Yabashi, T. Ishikawa, S. Suga, Y. Onuki, T. Ebihara, and A. Sekiyama, Probing strongly correlated 4*f*-orbital symmetry of the ground state in Yb compounds by linear dichroism in core-level photoemission, J. Phys. Soc. Jpn. **83**, 123702 (2014).

[50] A. Sekiyama, Y. Kanai, A. Tanaka, and S. Imada, Optical process of linear dichroism in angle-resolved core-level photoemission reflecting strongly correlated anisotropic orbital symmetry, J. Phys. Soc. Jpn. **88**, 013706 (2019).

[51] G. Stryganyuk, X. Kozina, G. H. Fecher, S. Ouardi, S. Chadov, C. Felser, G. Shonhense, P. Lushchyk, A. Oelsner, P. Bernhard, E. Ikenaga, T. Sugiyama, H. Sukegawa, Z. Wen, K. Inomata, and K. Kobayashi, Spin polarimetry and magnetic dichroism on a buried magnetic layer using hard X-ray photoelectron spectroscopy, Jpn. J. Appl. Phys. **51**, 016602 (2012).

[52] T. Matsushita, F. Matsui, H. Daimon, and K. Hayashi, Photoelectron holography with improved image reconstruction, J. Electron Spectrosc. Relat. Phenom. **178-179**, 195 (2010).

[53] S. Nemsak, M. Gehlmann, C.-T. Kuo, S.-C. Lin, C. Schlueter, E. Miynczak, T.-L. Lee, L. Plucinski, H. Ebert, I. Di Marco, J. Minar, C. M. Schneider, C. S. Fadley, Element- and momentum-resolved electronic structure of the dilute magnetic semiconductor manganese doped gallium arsenide, Nat. Commun. **9**, 3306 (2018).

[54] J. Chen, D. J. Huang, A. Tanaka, C. F. Chang, S. C. Chung, W. B. Wu, and C. T. Cheng, Magnetic circular dichroism in Fe 2*p* resonant photoemission of magnetite, Phys. Rev. B **69**, 085107 (2004).

[55] J. Garcia and G. Subias, The Verwey transition-a new perspective, J. Phys. Condens. Matter **16**, R145 (2004).

[56] J. Garcia, G. Subias, M. G. Proietti, H. Renevier, Y. Joly, J. L. Hodeau, J. Blasco, M. C. Sanchez,

and J. F. Berar, Resonant “forbidden” reflections in magnetite, Phys. Rev. Lett. **85**, 578 (2000).

[57] M. S. Senn, J. P. Wright, and J. P. Attfield, Charge order and three-site distortions in the Verwey structure of magnetite, Nature (London) **481**, 173 (2012).

[58] E. Baldini, C. A. Belvin, M. Rodriguez-Vega, I. O. Ozel, D. Legut, A. Kozlowski, A. M. Ples, K. Parlinski, P. Piekarz, J. Lorenzana, G. A. Fiete, and N. Gedik, Discovery of the soft electronic modes of the trimeron oeder in magnetite, Nat. Phys. **16**, 541 (2020).

[59] P. Piekarz, D. Legut, E. Baldini, C. A. Belvin, T. Kolodziej, W. Tabis, A, Kozlowski, Z. Kakol, Z. Tarnawski, J. Lorenzana, N. Gredik, A. M. Oles, J. M. Hoing, K. Parlinski, Trimelon-phonon coupling in magnetite, Phys. Rev. B **103**, 104303 (2021).

Figure captions

FIG. 1. (Color online) Depth-dependent Fe 2*p* core-level HAXPES spectra of the 150-nm-thick Fe_3O_4 thin film measured at (a) 300 K, (b) 150 K, and (c) 110 K. By tuning the X-ray attenuation length by θ_{in}, the spectra with λ_{eff} = 1.95, 3.76, and 7.33 nm (θ_{in} = 0.38, 0.51, and 2.00°, respectively) were obtained. The surface contribution-reduced spectra (λ_{eff} = 12.8 nm) were numerically obtained by Eq. (1) according to Ref. [17]. The spectra were normalized by the highest intensity in the Fe $2p_{3/2}$ region after subtracting an integrated-type background.

FIG. 2. (Color online) Enlarged view of the depth-dependent HAXPES spectra around the Fe $2p_{3/2}$ region measured at (a) 300, (b) 150, and (c) 110 K.

FIG. 3. (Color online) Valence band HAXPES spectra of the Fe_3O_4 thin film in the vicinity of E_F measured at (a) 300, (b) 150, and (c) 110 K for different λ_{eff}. The position of E_{on} for λ_{eff} = 14.0 nm determined by the extrapolation of the leading edge is indicated by the vertical bar in each figure. (d) *T*- and λ_{eff}-dependent E_{on} of the Fe_3O_4 thin film. The positive (negative) value indicates that the position of E_{on} is located below (above) E_F.

FIG. 4. (Color online) Fe 2*p* core-level HAXPES spectra at *T* = (a) 300, (b) 150, and (c) 110 K measured with RCP and LCP X-rays. The intensity difference between the RCP and LCP spectra corresponds to MCD-HAXPES. θ_{in} is set to 2.00° (λ_{eff} = 7.33 nm).

FIG. 5. (Color online) Calculated Fe 2*p* core-level HAXPES and MCD spectra for (a) *B*-site Fe^{2+}, (b) *B*-site Fe^{3+}, and (c) *A*-site Fe^{3+} components by using the electronic structure parameters shown in

Table I. (d) Calculated HAXPES with an integrated-type background (black solid line) and MCD spectra for Fe_3O_4 by using the spectra shown in (a), (b), and (c) with the ratio of 1 : 1 : 1. (e) Comparison of the experimental MCD spectra (T = 300, 150 , and 110 K) and the calculated MCD spectra.

FIG 6. (Color online) Calculated Fe 2*p* core-level XAS-MCD spectra for Fe_3O_4 by using the electronic structure parameters shown in Table I.

FIG. 7. (Color online) Comparison of the experimental and calculated Fe 2*p* core-level spectra. The experimental spectrum was obtained by the sum of the LCP and RCP spectra shown in Fig. 4(a). The calculated spectrum was also obtained by the sum of the spectra shown in Fig. 5(a)-(c).

Table

Table I. Electronic structure parameters for Fe_3O_4 used in the Fe 2*p* MCD-HAXPES and XAS-MCD calculations. The parameters are given in units of eV. In the octahedral (tetrahedral) site, the positive (negative) value of 10*Dq* is employed. An exchange field of +150 (-150) meV was applied to the *B*- (*A*-) site in the calculations.

Sites	10*Dq*	Δ	$V(e_g)$	$V(t_{2g})$	U_{dd}	U_{dc}
B-site (Fe^{2+})	1.6	7.0	2.0	1.0	6.0	7.5
B-site (Fe^{3+})	1.6	3.0	2.0	1.0	6.0	7.5
A-site (Fe^{3+})	-0.6	3.5	1.0	2.0	6.0	7.5

Figures

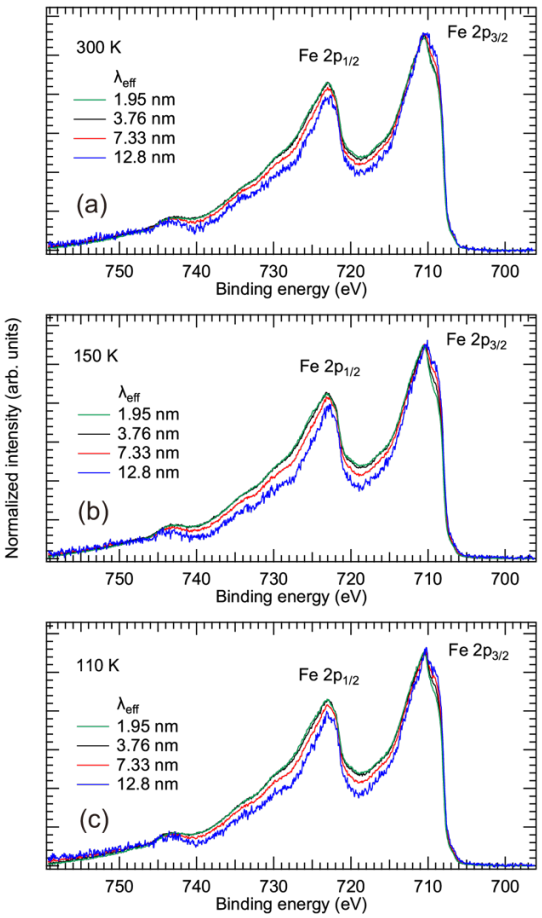


Figure 1

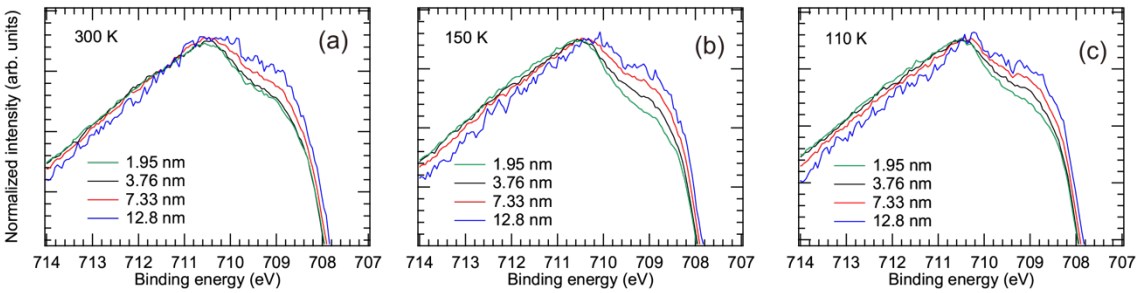

Normalized intensity (arb. units)
300 K
(a)
150 K
(b)
110 K
(c)
1.95 nm
3.76 nm
7.33 nm
12.8 nm
714 713 712 711 710 709 708 707
Binding energy (eV)

Figure 2

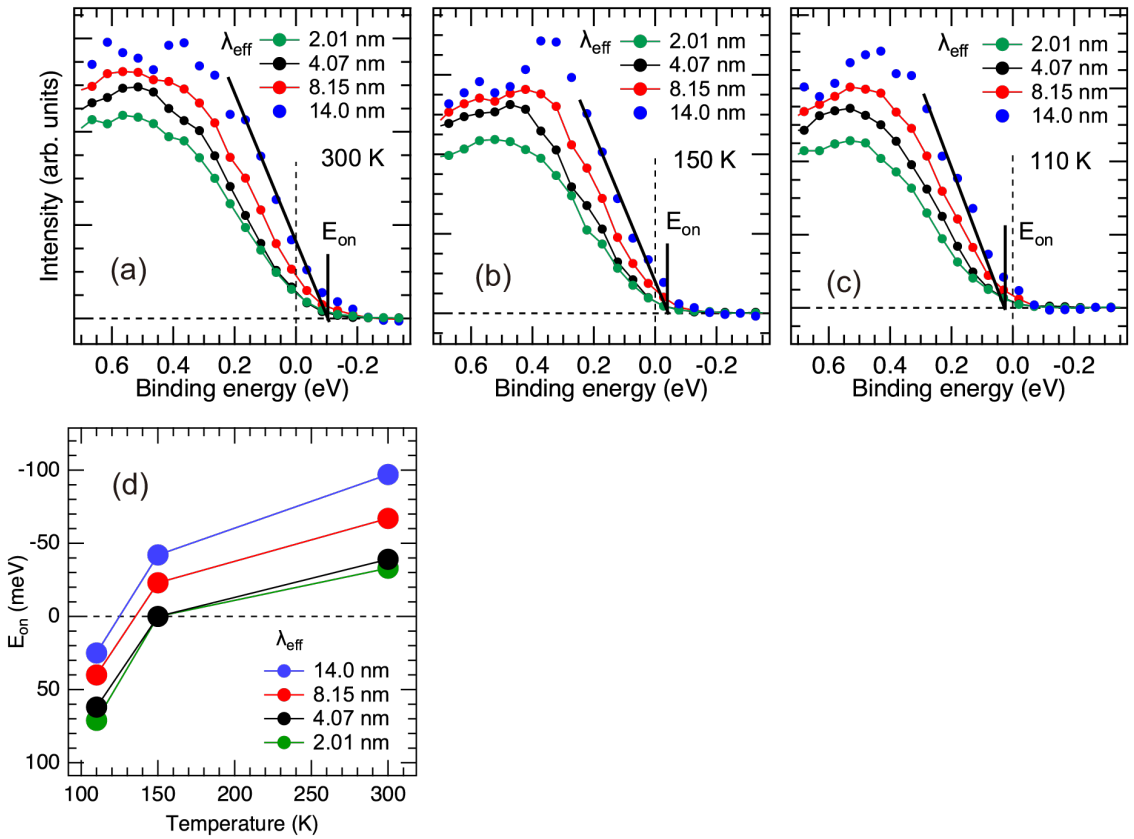

Intensity (arb. units)
λeff
2.01 nm
4.07 nm
8.15 nm
14.0 nm
300 K
Eon
(a)
0.6 0.4 0.2 0.0 -0.2
Binding energy (eV)
150 K
(b)
110 K
(c)
(d)
Eon (meV)
-100
-50
0
50
100
100 150 200 250 300
Temperature (K)

Figure 3

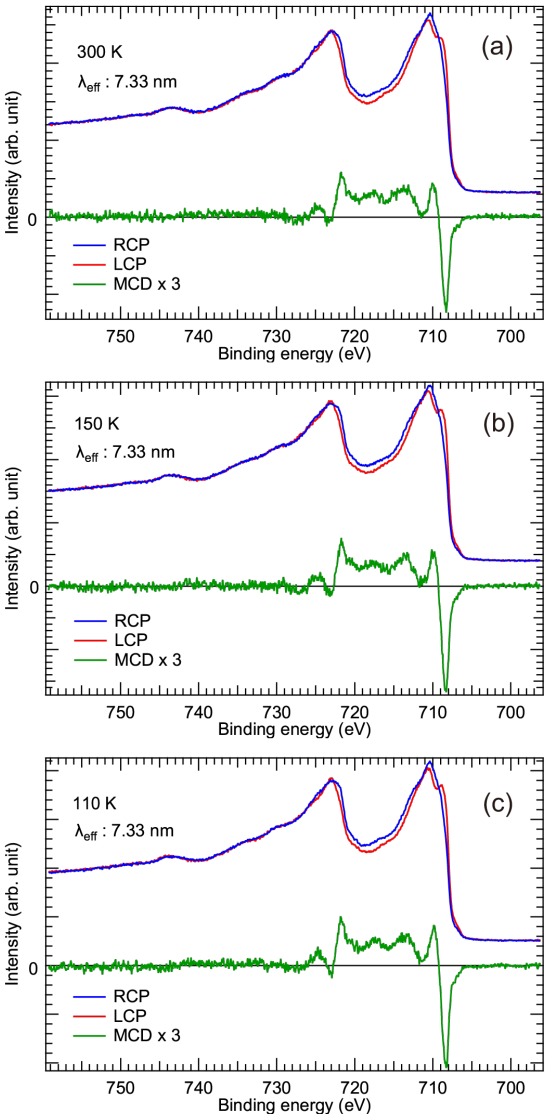

300 K
λeff : 7.33 nm
(a)
Intensity (arb. unit)
0
RCP
LCP
MCD x 3
750
740
730
720
710
700
Binding energy (eV)
150 K
λeff : 7.33 nm
(b)
Intensity (arb. unit)
0
RCP
LCP
MCD x 3
750
740
730
720
710
700
Binding energy (eV)
110 K
λeff : 7.33 nm
(c)
Intensity (arb. unit)
0
RCP
LCP
MCD x 3
750
740
730
720
710
700
Binding energy (eV)

Figure 4

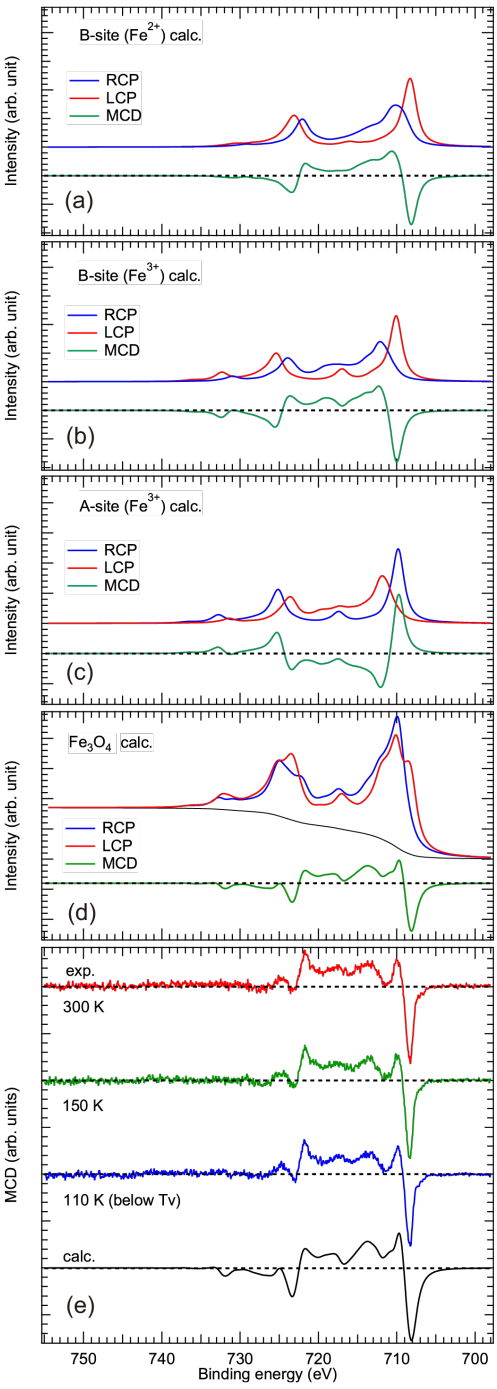

B-site (Fe2+) calc.
RCP
LCP
MCD
(a)
B-site (Fe3+) calc.
RCP
LCP
MCD
(b)
A-site (Fe3+) calc.
RCP
LCP
MCD
(c)
Fe3O4 calc.
RCP
LCP
MCD
(d)
exp.
300 K
150 K
110 K (below Tv)
calc.
(e)
Intensity (arb. unit)
MCD (arb. units)
750
740
730
720
710
700
Binding energy (eV)

Figure 5

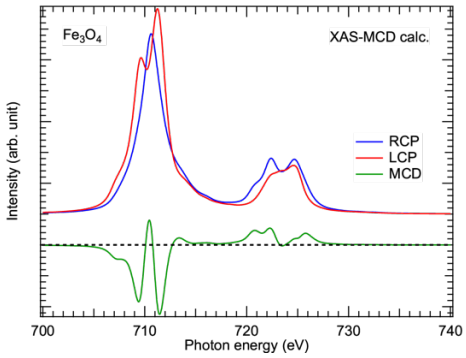

Fe3O4
XAS-MCD calc.
RCP
LCP
MCD
Intensity (arb. unit)
700
710
720
730
740
Photon energy (eV)

Figure 6

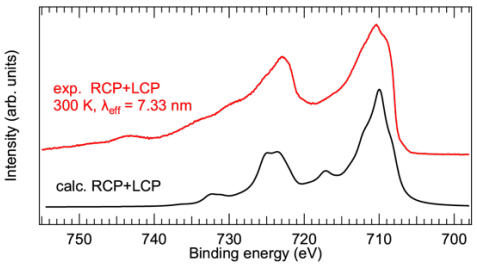

exp. RCP+LCP
300 K, λeff = 7.33 nm
calc. RCP+LCP
Intensity (arb. units)
750
740
730
720
710
700
Binding energy (eV)

Figure 7